# CHAPTER 1

# MINERALOGY OF TALC

## 1.1- Research objectives

Surface free energies and its components between two interacting surfaces are critically important in a number of industrial applications including adhesion, coating, printing, de-inking, lubrication, compounding; and have an influence on daily life, biology and chemistry [1-3]. Many of the mineral processing techniques, e.g. flotation, selective flocculation and filtration also depend on the interfacial interactions between solid and liquid, essentially water [4]. These interactions are mainly controlled by the interfacial surface free energy between two phases, which dictates the strength of interaction.

Talc is a very versatile mineral used in many industrial applications due to mainly its unique surface chemistry and lamellar crystal habit. Cosmetics, pharmaceuticals, paints, polymers, ceramics and paper are a few examples of market segments where the interfacial interactions between the talc's surface and its environment dictate the ultimate performance of the mineral. The characterization of the surface properties and especially the surface free energy components of talc are, therefore, recognized as the key to understanding the mechanism of surface-based phenomena since it provides essential insight into the fundamental principles of such interactions. In addition, the knowledge of the geometrical properties of the anisometric particles, namely the aspect ratio, is also of paramount importance since it plays a key role in the final performance of the mineral in many industrial applications such as polymer reinforcement, paper coating, and gas barrier among others [5-8].

In a broad view, what is aimed herein is a comprehensive surface thermodynamic and geometrical characterization of 8 different powdered talc samples. More specifically speaking, the purpose of the present work is four-fold:

- Determine the contact angle of different liquids with flat and powdered talc samples and make a preliminary comparison of different contact angle techniques (Chapter 3);

- Characterize the surface thermodynamic properties of talc using the acid-base theory for solids (Chapters 2 and 3);

- Determine the aspect ratio of talc powders using particle size distribution methods (Chapter 4);

- Determine the percentage of hydrophobic and hydrophilic sites and the surface free energy components at basal and edge surface of talc using flow microcalorimetry (Chapter 5).

The rest of Chapter 1, that follows, deals with the mineralogical aspects of talc that are of relevance for a better understanding of the mineral's surface chemistry and physical properties.

## 1.2- Introduction and background

The name talc is probably derived from the Arabic *talk*, for pure, most likely referring to talc's white color [9]. A massive talcose rock, often with admixed serpentine and calcite, is called steatite, and an impure massive variety is known as soapstone. The latter name is in reference to the "soapy" feel, the former from the Greek through the Latin *steatitis,* precious stone.

Talc, a naturally occurring mineral, is a crystalline hydrated magnesium silicate and in its pure form has the unit cell chemical formula $[Si_4](Mg_3)O_{10}(OH)_2$ [10], where the cation enclosed in brackets is in tetrahedral coordination and that enclosed in parentheses is in octahedral coordination. In terms of oxides, the chemical formula can be written as $3MgO.4SiO_2.H_2O$ and the theoretical chemical composition shows the following values (% w/w):

$SiO_2$ – 63.37%
MgO – 31.88%
$H_2O$ – 4.75%
(present as crystalline water)

Talc is a *sui generis* raw material due to its properties which make its uses so diversified. It is widely used commercially because of its lamellar habit, softness, whiteness, fragrance retention, luster and chemical purity. Other commercially important properties of talc are its chemical inertness, low abrasion, high thermal conductivity and stability, low electrical conductivity, and high oil and grease adsorption [11, 12]. The chemical properties of talc's surface control many industrial processes that utilize this mineral and are largely derived from its crystal structure and chemical composition. A better understanding of both talc's properties and surface chemistry/functionality requires the explanation of some mineralogical concepts, which follow.

## 1.3- Clay minerals - definition

The terms "clay" and "clay mineral" are used in very different contexts. For example, a common interpretation of a clay substance is a material whose constituent particles are very small, with an average equivalent diameter smaller then 2 μm, the "clay fraction". This is typically an engineering and sedimentological usage. It is only very recently that clay mineralogists have agreed on meanings for the two terms [13]. The term "clay" now refers to a "naturally occurring material composed primarily of fine-grained materials, including crystalline and amorphous oxides and hydroxides of various metals [14], which are generally plastic at appropriate water contents and will harden when dried or fired". The term "clay mineral" refers to a certain group of lamellar or layered crystalline silicate minerals, the phyllosilicates.

According to Bailey [15], the phyllosilicate minerals fall into seven groups: Serpentine-kaolin, Talc-pyrophyllite, Smectite, Vermiculite, True mica, Brittle mica and Chlorite. The main minerals belonging to the talc and pyrophyllite group are listed in Table 1.1.

**Table 1.1. Pyrophillite-Talc group of minerals. Adapted from [9]**

| Mineral | Chemical formula | Space Group | a (Å) | b (Å) | C (Å) | $\alpha$ (°) | $\beta$ (°) | $\gamma$ (°) |
|---|---|---|---|---|---|---|---|---|
| Pyrophyllite | $Al_2Si_4O_{10}(OH)_2$ | $C\bar{1}$ | 5.160 | 8.966 | 9.347 | 91.18 | 100.46 | 89.64 |
| Pyrophyllite | $Al_2Si_4O_{10}(OH)_2$ | C2/c | 5.138 | 8.910 | 18.60 | | 100.02 | |
| Ferripyrophyllite | $Fe_2^{3+}Si_4O_{10}(OH)_2$ | C2/m | 5.26 | 9.10 | 19.1 | | 95.5 | |
| Talc | $Mg_3Si_4O_{10}(OH)_2$ | $C\bar{1}$ | 5.290 | 9.173 | 9.46 | 90.46 | 98.68 | 90.09 |
| Willemseite[a] | $(Ni,Mg)_3Si_4O_{10}(OH)_2$ | C2/c or Cc | 5.136 | 9.149 | 18.994 | | 99.96 | |

[a] **Willemseite is a variety with nickel as the major octahedral cation [16].**

## 1.4- Silicate mineral structures: Pauling's polyhedral paradigm

The general character of the atomic structure of the most clay minerals was developed in the 1930's on the basis of general structural relationships of layer silicate minerals, as determined by Pauling [17-19].

In simplest terms, silicate minerals can be considered inorganic polymers based on two basic "monomer" structures. These are the tetrahedron and the octahedron of Figure 1.1, which represent the placement of oxygen atoms (the apices of the polyhedron) and the smaller cations (at the centers of the polyhedron). The multitude of clay minerals stoichiometries are built basically from these two building blocks [3].

Many of the silicates can be pictured as the configurations made by joining of such tetrahedra and octahedra to themselves and to each other in three dimensions. These involve the sharing of corners, edges, and faces in numerous conformations. Since the corners of coordination polyhedra are typically oxygen atoms, corner sharing simply means that a (single) shared oxygen atom is coordinating two neighboring cations [20]. Similarly a shared edge represents two oxygen atoms which both belong to adjacent coordination polyhedra. These two aspects of mineral crystal structures are shown in Figure 1.2 for tetrahedra and octahedra.

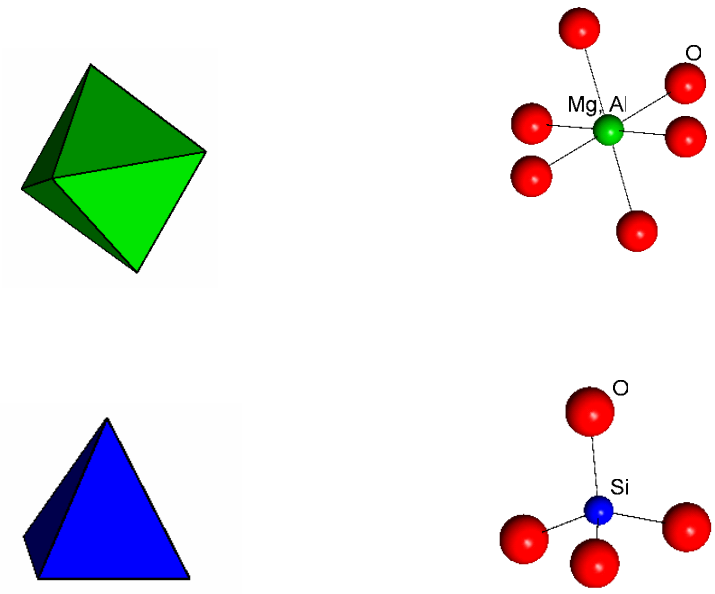


**Figure 1.1. Polyhedra (left) and the corresponding atomic arrangement (right) for the two principal polyhedra of silicate mineral structures, i.e., octahedron (upper) and tetrahedron (lower).**

The possible geometric permutations are further modified by chemical substitutions within the structure, which usually depend on how well a metal ion will fit among close-packed oxygen ions. This is largely a matter of relative ionic radii. Given an $O^{2-}$ ionic radius of 1.40Å [21], the preferred (most stable) coordination of cations common in industrial silicate minerals has been calculated and expressed in terms of ionic radius ratio, as shown in Table 1.2. As Table 1.2 suggests, like-size cations can and do substitute for the theoretical components in nature. Two divalent cations which are not very different in ionic radius, magnesium and iron, for example, can readily substitute for each other in an octahedral site. The phenomenon is called isomorphous substitution [22] and can be defined as “the replacement of one atom by another of similar size in a crystal structure without disrupting or seriously changing the structure” [23]. A more detailed discussion about the other possible substitutional types present in silicates was discussed elsewhere [24] .

**Table 1.2. The most commonly observed coordination polyhedra for the common elements in silicate structures in order of decreasing amount in the Earth's crust, omitting oxygen which is the most abundant element. Adapted from refs. [3, 25]**

| Ion | Ionic radius (Å) | Coordination number | Polyhedron | $R_M:R_O$ |
|---|---|---|---|---|
| $Si^{4+}$ | 0.26 | 4 | Tetrahedron | 0.186 |
| $Al^{3+}$ | 0.39<br>0.535 | 4<br>6 | tetrahedron<br>octahedron | 0.279<br>0.382 |
| $Fe^{2+}$ | 0.78<br>0.61 | 6<br>6 | octahedron<br>cube | 0.557<br>0.436 |
| $Ca^{2+}$ | 1.00<br>1.12 | 6<br>8 | octahedron<br>cube | 0.714<br>0.800 |
| $Na^{1+}$ | 1.02<br>1.18 | 6<br>8 | octahedron<br>cube | 0.728<br>0.843 |
| $K^{1+}$ | 1.38<br>1.51 | 6<br>8 | octahedron<br>cube | 0.986<br>1.079 |
| $Mg^{2+}$ | 0.72<br>0.89 | 6<br>8 | octahedron<br>cube | 0.514<br>0.636 |

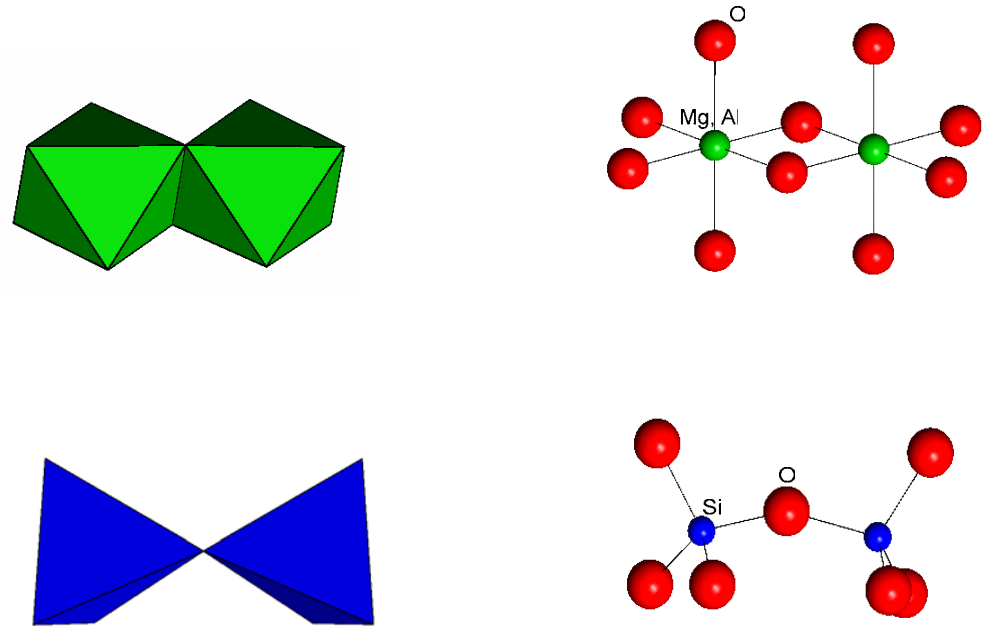


**Figure 1.2. The polyhedral (left) and equivalent atomic arrangement (right) illustrating two common modes of sharing between polyhedra. The upper diagrams show two octahedra sharing an edge (two oxygen atoms) and the lower diagrams show two tetrahedra sharing a corner (a single oxygen atom).**

## 1.5- Structure of Phyllosilicates

### 1.5.1- Layer types

As the name indicates, phyllosilicate (from the Greek, phyllon, a leaf, as in a leaf of a plant) minerals are layer structures [3]. That is, ideally the atomic arrangement contain continuous two-dimensional tetrahedral sheets of composition $T_2O_5^{-2}$ (T = tetrahedral cation, normally $Si^{4+}$, $Al^{3+}$, $Fe^{3+}$), in which individual tetrahedra are linked with neighboring tetrahedra by sharing three corners each (the basal oxygens atoms) to form a pseudo-hexagonal (ditrigonal) mesh pattern [26], known as siloxane ditrigonal cavity [20]. As shown in Figure 1.3a, there is a net negative charge on a sheet of tetrahedra as found in phyllosilicate minerals. This charge can be balanced by the addition of other cations, and, in phyllosilicates, this is done by the addition of a sheet of octahedra (O). Consequently, at the unshared corners of the tetrahedra, i.e. the fourth corner, the apical oxygen atoms point in the same direction to form part of an immediately adjacent octahedral sheet in which individual octahedral are linked laterally by sharing octahedral edges. This oxygen sharing occurs in the crystallographic ***c*** direction of the tetrahedral sheet structure[1] (Figure 1.3b). The two sheets thus form a layer, the assemblage being given by the name "1:1" or “T-O”, as in 1 tetrahedral layer and 1 octahedral layer. The exposed surface of the octahedral sheet in 1:1 type minerals consists of OH groups. This type of layer is found, for example, in kaolinite[2].

[1] The bridging of the tetrahedral with the octahedral sheets always produces a significant distortion in the final layer structure caused by the fact that the apical oxygens cannot fit into vertices of the octahedra to form a layer and still preserve the ideal hexagonal pattern of the tetrahedra. This geometric restriction lowers the symmetry of the cavities in the basal plane of the tetrahedral sheets from hexagonal to trigonal. As another result, the basal surface becomes less planar (slightly corrugated) [13].
[2] Kaolinite is known commercially as kaolin.

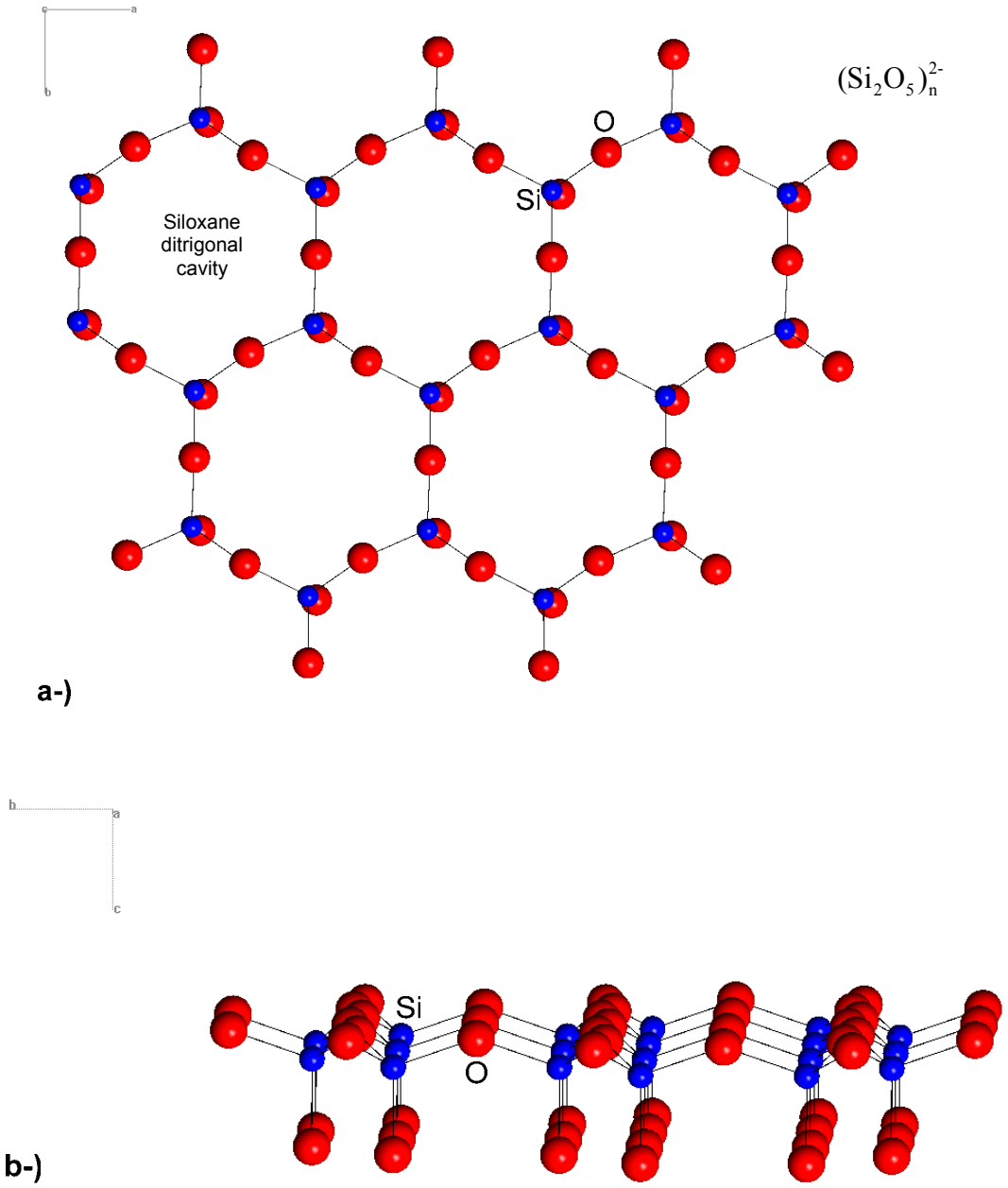


**Figure 1.3. The tetrahedral polymerized sheet characteristic of phyllosilicates. The six-membered rings of the tetrahedral layer have nearly hexagonal symmetry (ditrigonal). a) View down the *c* axis, b) View down the *a* axis.**

Rather than terminate the external plane of oxygen atoms of the octahedral sheet by hydroxyl groups, as in the 1:1 minerals, it is possible to add a second tetrahedral sheet, this one inverted with reference to the first tetrahedral sheet, making a 2:1 or T-O-T mineral structure, which is the case of talc, pyrophyllite, mica, smectite and others. Here the "2" refers to the number of tetrahedral sheets and the "1" refers to the number

of octahedral sheets. Finally, there are layer structures which have octahedral (hydroxide) sheets inserted between 2:1 type layers. These are labeled 2:1:1 or T-O-T-O. Chlorite is a mineral belonging to this class. Clearly, as the complexity of the layer increases, the thickness of the layer, which can be measured by X-ray, also increases. Because the nature of the layer is so directly reflected in the thickness of the layer, the clay types 1:1, 2:1 and 2:1:1 are also referred to as the 7Å, 10Å and 14Å groups respectively [24], where the thickness represents the stacking of identical layers with no water or other molecular species occupying the interlayer region in the crystallographic ***c*** direction.

The gap separating each layer is termed interlayer space or gallery. Mechanically, the layers are more strongly bonded than the interlayers so that cleavage will preferentially occur along the interlayer regions. The stronger and more specific the interlayer bond is, generally, the more regular and perfect will be the stacking. This is typically the situation encountered with the mica group of minerals. Conversely, the weaker and more diffuse the interlayer bonding, the less regular the stacking, the greater the number of stacking faults, and ultimately, one has a near-random stacking which is termed "turbostratic" [27]. Such is the case for many clay minerals, particularly for the smectite group of minerals.

### 1.5.2- Octahedral site occupancy

While all the tetrahedral sites are occupied in these structures, such is not necessarily the case for the octahedral sites. When the octahedra contain a divalent ion such as $Mg^{2+}$ and $Fe^{2+}$, charge balance between the sheets is achieved when all sites are occupied, as illustrated in Figure 1.4a. As there are three octahedra within each hexagonal ring of tetrahedra, the sheet is termed a trioctahedral sheet. When a trivalent ion such as $Al^{3+}$ or $Fe^{3+}$ occupies the octahedra, only two thirds of the octahedra are occupied, as shown in Figure 1.4b, and the sheet is termed a dioctahedral sheet [3]. The occupied octahedra in a dioctahedral sheet are invariably

more distorted and the vacant site is significantly larger than the occupied sites around it.

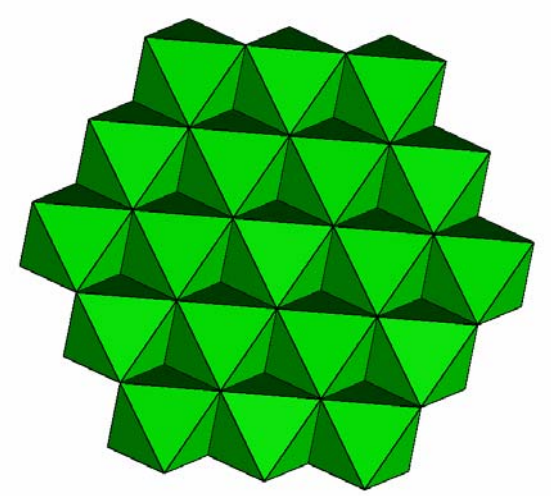

(a) Trioctahedral

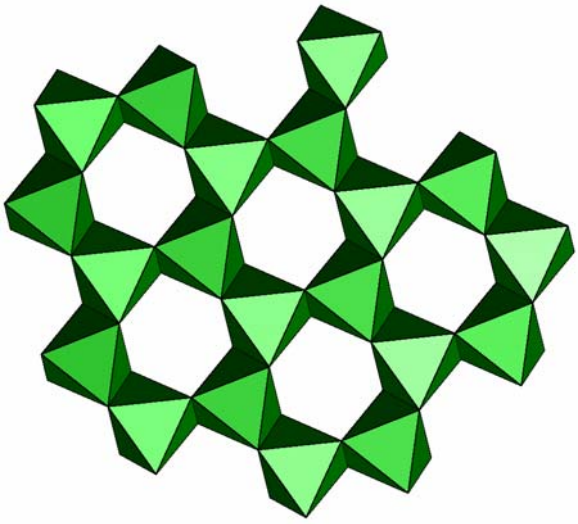

(b) Dioctahedral

**Figure 1.4. Octahedral sheets for the trioctahedral (a) and dioctahedral cases (b). Note that the existence of the vacant octahedral site (b) creates distortions in the remaining octahedral sites and an enlargement of the octahedral site which is missing the cation.**

### 1.5.3- Layer charge

The layer charge, represented by X, is considered an especially important characteristic of 2:1 phyllosilicates. The layer charge indicates a mineral's capacity to retain cations and to adsorb water and various polar organic molecules and is directly related to the interlamellar cation exchange capacity (CEC), measured in mmole/g [28, 29]. The

concept of CEC is of very importance in soil science and further information can be found in the comprehensive work of McBride [30]. The term layer charge refers to an excess of (usually) negative charge per formula unit that may exist on certain phyllosilicates [15] . A net negative charge can arise from:

- substitution of $R^{3+}$ or $R^{2+}$ for $Si^{4+}$ in tetrahedral coordination;
- substitution of $R^{1+}$ or $R^{2+}$ for $R^{2+}$ or $R^{3+}$, respectively, in octahedral coordination;
- presence of octahedral vacancies, or
- dehydroxylation of OH to $O^{-}$.

The net charge may originate entirely within the tetrahedral sheet or entirely within the octahedral sheet in some species, or may come partly from both sheets. Whatever the source of negative charge, its magnitude must be balanced by a corresponding positive charge on the interlayer so that the crystal as a whole is electrostatically neutral.

It is not surprising that the magnitude of the layer charge, and secondarily the site of the charge, can influence the chemical and physical properties of the phyllosilicate minerals, although it is frequently difficult to quantify this. The layer charge characteristic of phyllosilicates was thoroughly discussed elsewhere [29].

### 1.5.4- The interlayer

The interlayer bonding for the 1:1 layer silicates, whether dioctahedral or trioctahedral, is via hydrogen bonds from one hydroxyl surface to the adjacent oxygen plane of the neighboring 1:1 layer. These are long hydrogen bonds, but there are many of them and thus their contribution to the interlayer bonding is strong. Any ionic substitution occurring in the 1:1 layer is usually such that overall electrostatic neutrality is maintained, i.e., the layer charge is always zero or very near to zero [3].

The 2:1 layer is more complex because it is possible to have a net layer charge. Since such a situation would be unstable because of the electrostatic repulsion between all the layers, the charge must be balanced by the presence of extra positive charge. There is no site in the layer for the placement of this charge (e.g., extra cations), but the positively charged entities easily can be situated between the layers. This creates an alternating arrangement of ...layer-interlayer-layer-interlayer... where the electrostatic charges also alternate, i.e., negative-positive-negative-positive.

There are basically four types of interlayer moiety commonly encountered in naturally occurring materials and as modified materials. These are:

1) a vacancy (for a zero-charge layer)
2) a cation (e.g., $Na^{1+}$, $Ca^{2+}$)
3) an inorganic complex (e.g., a positively charged hydroxide sheet as in the 2:1:1 chlorite structure)
4) a organic cation (e.g., a quaternary ammonium cation in a modified material).

The minimum layer charge is zero and the maximum is 2 (this is the negative charge per formula unit). Because the chemical and physical properties are strongly influenced by the layer charge, the magnitude of the charge is a major factor in the classification of the different types of 2:1 minerals. Table 1.3 shows this classification.

## 1.6- Surface functional groups in phyllosilicates

Surface functionality refers to the chemical functional groups that terminate the bulk structure of the solid and their immediate environment. In inorganic clays the two most important surface functional groups are the siloxane ditrigonal cavity and the hydroxyl groups [20], i.e., the 001 basal planes and the edges, respectively.

**Table 1.3. The classification of the phyllosilicates minerals based on layer type, the nature of the octahedral sheet and the magnitude of the layer charge. For each group, a common mineral or group of minerals are listed**

| Layer type | Interlayer occupancy (X = layer charge) | Dioctahedral | Trioctahedral |
|---|---|---|---|
| 1:1 | None (water) $X \approx 0$ | Kaolinite | Serpentine |
| 2:1 | None $X \approx 0$ | Pyrophyllite | Talc |
| | Hydrated cations $X \approx 0.2 – 0.6$ | Smectites | |
| | Hydrated cations $X \approx 0.6 – 0.9$ | Vermiculites | |
| | Cations $X \approx 1$ | (true) micas | |
| | Cations $X \approx 2$ | (brittle) micas | |
| 2:1:1 | Hydroxide sheet variable X | Chlorites 2:1:1 | |

### 1.6.1- The siloxane surface reactivity

The surface reactivity of any solid derives from the chemical behavior of surface functional groups. The plane of oxygen atoms (basal plane) formed at the tetrahedral silica sheet is called a siloxane surface. This plane is characterized by a distorted hexagonal (ditrigonal) symmetry among its constituent oxygen atoms that is produced when the tetrahedral layer is connected to the octahedral layer by sharing their apical oxygens.

A reactive site associated with this surface is the ditrigonal cavity formed by the bases of six corner-sharing Si tetrahedra. This cavity has a diameter of 0.26 nm and is bordered by six sets of lone-pair electron orbitals emanating from the surrounding ring of oxygens atoms [20]. These structural features qualify the ditrigonal cavity as a Lewis base, which is any molecular unit that uses a doubly occupied electron orbital in initiating a chemical reaction [31], in this case as an electron donor.

Lindgreen and co-workers [32], when studying the surface morphology of smectite clays by atomic force microscopy (AFM), took what was claimed to be the first atomic resolution image of a silicate surface (Figure 1.5). Similar images were obtained lately by Henderson *et al.* [33].

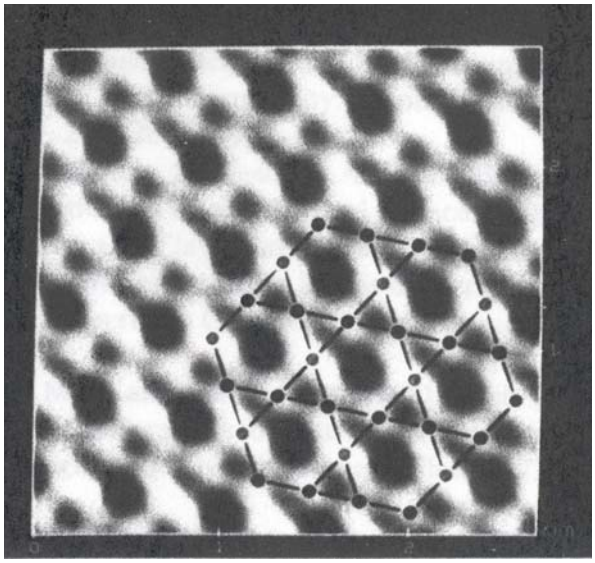

**Figure 1.5. Atomic force microscope image of the surface of illite/smectite. The inserted model shows the arrangement of O atoms on the surface of the tetrahedral sheet. The scan area is 2.6 x 2.6 nm. The contours on the surface could represent the ditrigonal O surface of the tetrahedral sheet of the 2:1 layer silicate. Reprinted with permission from ref. [32].**

The reactivity of the siloxane ditrigonal cavity depends on the nature of the local electronic charge distribution. If there are no isomorphic cation substitutions to create deficits of positive charge in the underlying layer, the ditrigonal cavity functions as a very soft Lewis base. This is, ideally, the case of pure talc and pyrophyllite.

If isomorphic substitution of $Al^{3+}$ by $Fe^{2+}$ or $Mg^{2+}$ occurs in the octahedral sheet, the resulting excess negative charge spreads itself principally over 10 surface oxygen atoms of the four silica tetrahedra that are associated through their apexes with a singe octahedron in the layer. This distribution of negative charge enhances the Lewis base character of the ditrigonal cavity and makes it possible to form reasonably strong complexes with cations and water molecules.

On the other hand, if isomorphic substitution of $Si^{4+}$ by $Al^{3+}$ occurs in the tetrahedral sheet, the excess of negative charge is localized much nearer to the periphery of the siloxane surface and it has to be divided only by the three surface oxygen atoms of one tetrahedron. Consequently, much stronger complexes with cations and dipolar molecules become possible because of this localization of charge [22].

At the solid/aqueous solution interface this negative charge that arises from isomorphic substitution is pH independent. The model is known as the constant basal surface charge model [34].

The wettability of the oxygen basal plane of phyllosilicates was discussed by Yariv [35] in terms of hybridization of the oxygen orbitals, which in turn determine the angle of the bong Si–O–Si in the tetrahedral sheet. Determination of Si–O–Si angles in different silicates showed that this angle ranges between $120^{o}$ and $180^{o}$. According to that author, the hydrophobicity of the basal plane increase with the increasing of the Si–O–Si angle. In fact Si–O–Si angles of $136^{o}$ and $120^{o}$ have been observed for pyrophyllite and mica respectively, which are examples of hydrophobic and hydrophilic minerals [36, 37]. For silica, a value of $120^{o}$ was also reported [38]. Yariv also determined quantitatively the surface of basicity the oxygen planes of various clay minerals [39, 40]. A very detailed discussion about the chemical aspects of the Si–O–Si bond in silicates is depicted in the work of Liebau [41].

### 1.6.2- The hydroxyl group

When an alumino- or magnesium-silicate layer is disrupted, e.g. during grinding, a diversity of functional groups is exposed. Since they were in the interior of the crystal, the valences of these new functional groups are not completely satisfied causing them to be very reactive and they may react as electron pair donors (Lewis base) or acceptors (Lewis acid). These surfaces are called broken-bond surfaces or edge surfaces [14].

The surface properties of the edges depend greatly on the exposed atoms. That part of the surface at which the octahedral sheet is broken may be compared to the surface of gibbsite ($Al(OH)_3$) or brucite ($Mg(OH)_2$), whereas that part of the surface at which the tetrahedral sheet is broken may be compared to that of silica.

Typically, when the edge surfaces are exposed to atmosphere, they adsorb water molecules (chemisorption) and become covered with amphoteric surface hydroxyls, mainly in the form of silanol [–Si-OH], aluminol [–Al-OH] and magnesol [–Mg-OH] groups [14]. This process is schematically shown in Figure 1.6 and it helps to explain why the water content of clay increases with increasing time of grinding.

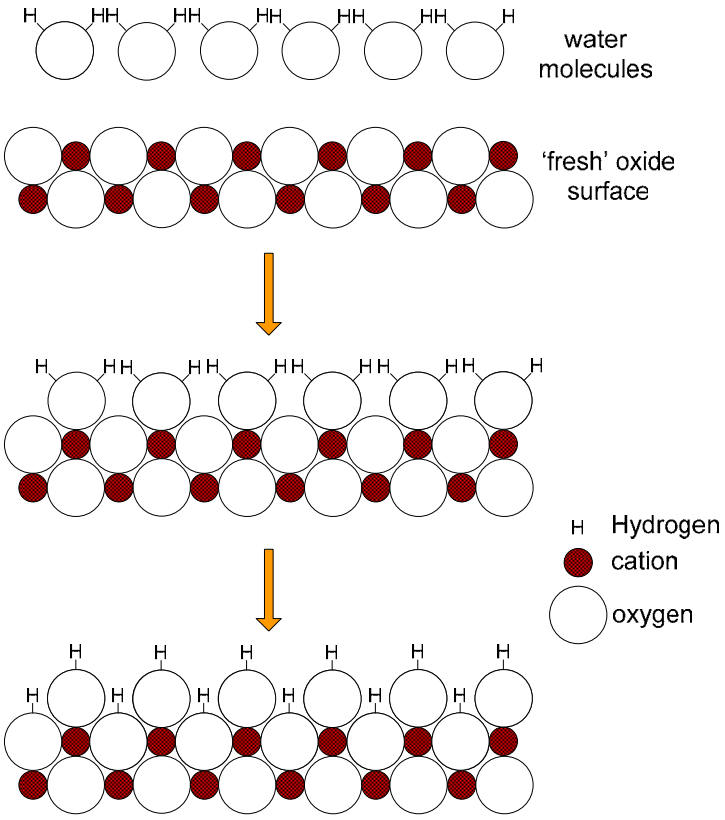


**Figure 1.6. Stepwise dissociative chemisorption of water at freshly cleaved oxides surfaces. I) The water molecules are attracted by the freshly cleaved oxide surfaces. II) The metal ions first coordinate the water molecule. III) Water dissociation occurs and the surface becomes covered with hydroxyl groups (hydroxylation). Adapted from [42, 43].**

When in aqueous solution, the reactivity of the OH groups does differ depending on the accompanying cation. The acid strengths, expressed in $pK_a$ values of OH groups on the oxides MgO, $Al_2O_3$ and $SiO_2$ are 18.5, 8.5, 7.0, respectively. As a quick reminder, the lower the p$K_a$, the stronger the acid. Strong acids have p$K_{as}$ of zero or less, while those of weak acids are positive[3]. For example, hydrochloric acid (HCl), a strong acid, has p$K_a$= -3 [21]. Therefore, the [–Mg-$O^-$] functional group is the first site to by protonated in the presence of water, followed by the octahedral [–Al-$O^-$], tetrahedral [–Al-$O^-$], and [–Si-$O^-$] groups, respectively. The [–Mg-OH] and [–Al-OH] can be further protonated at pH below 4 [14].

Clay minerals are widely titrated by acids and bases. Potentiometric titrations reveal that the charge of the edge surface depends on the pH and behave like amphoteric oxides, i.e. they can behave like acids or bases depending on the circumstances. It is assumed that the edge surfaces are the principal sites for acid-base reactions to take place in clay minerals. A typical potentiometric titration of talc is shown in Figure 1.7.

Figure 1.7 shows that a negative surface charge originates from acidic dissociation (deprotonation) of the surface hydroxyl groups (at pH > I.E.P) and increases with increasing with increasing pH. At pH < I.E.P., the magnesol groups become doubly protonated and the reversal of charge is observed.

The OH groups bonded to silicon (silanol) do not have an amphoteric behavior, because of the greater valence of the silicon. The oxygen atom cannot accommodate more than one hydrogen in this case. The net charge of this group can only be negative.

[3] Whether a compound of the general type M–O–H will act as an acid or a base depends in the final analysis on the relative strengths of the M–O and the O–H bonds. If the M–O bond is weaker, then the –OH part will tend to retain its individuality and will act as a hydroxide ion. If the O–H bond is weaker, the MO– part of the molecule will remain intact and the substance will be acidic.

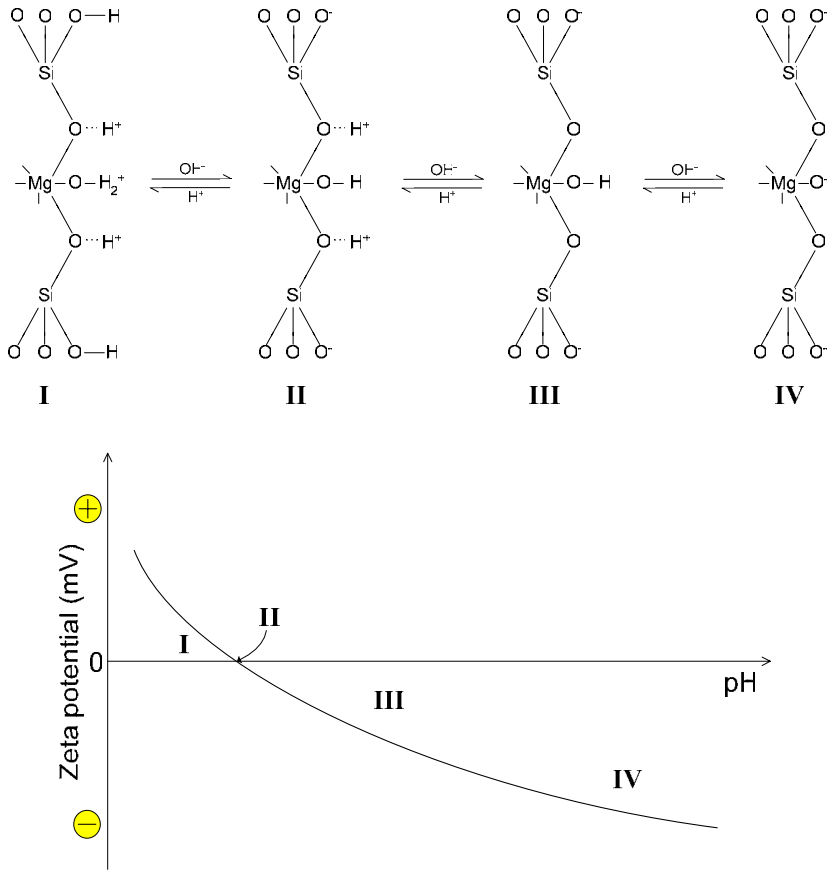


**Figure 1.7. A schematic representation of functional groups on the broken bond surface of talc as a function of pH of an aqueous talc suspension: (I) pH < 2; (II) Neutral complex at the isoelectric point (iep) of talc; (III) pH slightly above the iep; (IV) pH > 12.**

For silica, the surface hydroxyl groups are characterized by weak acidity, where the acid dissociation constant of is estimated to be ~$10^{-7}$ [44, 45]. Protonation of [–Si-$O^-$] appears of very low probability; the proton association constant for the reaction:

$$Si-OH \overset{H^+}{\rightleftharpoons} Si-OH_2^+$$

is characterized by a log *K* = -4.0 [46, 47], which indicates how low the probability of surface silanol protonation is. The estimated *K* for the protonation

of the siloxane link[4] [-Si–O–Si-] is even lower, log *K* = -16.9, which means that this group can be considered inert with respect the process of protonation [48].

The magnesol groups at the talc's edges, [–Mg-OH], in turn, have a dominantly moderate to strong basic character [49, 50] .

In the light of above considerations, the global functionality of the surface of a given mineral is largely dependent on the chemistry of the mineral, i.e. the degree of isomorphic substitution within the lattice and on the degree of physical disintegration of the clay mineral crystal. This latter factor, in the case of talc, determines the ratio **basal/edge** surfaces or the aspect ratio of the mineral and ultimately the ratio of the **hydrophobic ditrigonal cavities/hydrophilic edge hydroxyl groups,** which show dual character with respect to acid/base properties depending upon the pH of the medium. The hydrophobicity of the basal planes of talc is explained in the coming sections.

## 1.7- Talc properties

### 1.7.1- Crystal structure

Ideally talc and pyrophyllite are the only electrostatically neutral (X=0) 2:1 clay minerals. Talc is trioctahedral and pyrophyllite is dioctahedral [9].

Thus, talc's structure is based on T-O-T (tetrahedral-octahedral-tetrahedral) layers. According to Gehring [51], two arrangements of OH groups with respect to the cations in the octahedral sheet are possible (Figure 1.8a). In one type of site (M2 site), the two OH groups are arranged in a *cis* position, whereas in the other type (M1 site) a *trans* position occurs (Figure 1.8b). Over the average talc structure, the *cis* form is more frequent by a factor of two. All M sites are occupied by divalent ($Mg^{2+}$) cations. Two tetrahedral and one octahedral sheet give a 9.5Å thick unit-layer structure [52]. The

[4] The siloxane link is the surface functional group associated with the basal plane of the phyllosilicates.

stacking of successive T-O-T layers is shifted by approximately 0.3*a* along one of the pseudohexagonal axes, so that “hexagonal” rings in successive layers are not aligned. This arrangement provides the minimum amount of O–O and Si–Si repulsion, while maximizing attractive Si–O interactions between adjacent layers [53]. The interlayer space was estimated as 0.1Å [52].

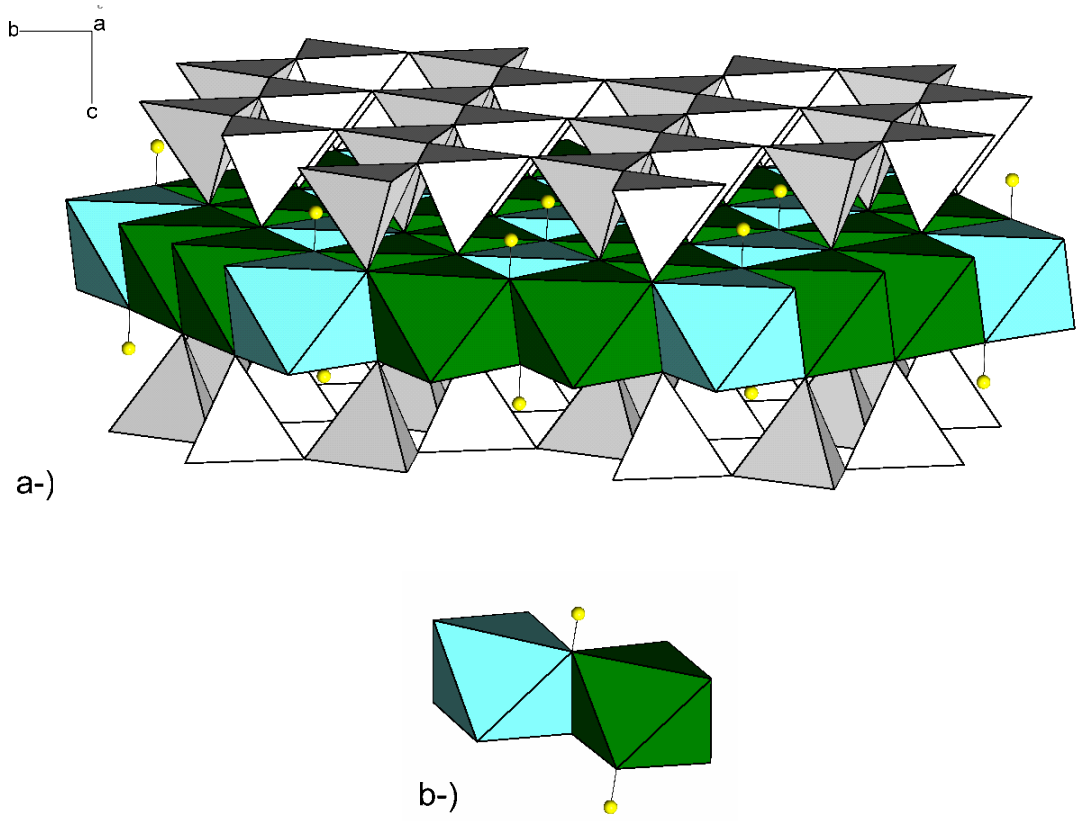


**Figure 1.8. (a) Talc structure (small spheres indicate hydroxyl groups) with the two types of octahedral sites (shaded differently); *(b) cis* and *trans* coordination of two octahedral sites marked in (a).**

The crystal structure of talc is illustrated in Figure 1.9. The fractional coordinates of atomic positions in the unit cell of talc used for creating the crystal structure are listed in Appendix 1.

Normally, it is reasonably pure compound with little substitution by other elements. Thus, the layer charge is zero (electrostatically neutral) or very small and the

layers are held together by a combination of predominantly Lifshitz-van der Waals forces (17.1 kcal/mole) [54-56] along with a minor net ionic attraction (maximum of 4.1 kcal/mole), in spite of the insignificant layer charge [57]. These are normally thought of as weak forces, yet there is no report in the literature describing the intercalation of water or any sort of organic molecular species between the talc layers. Due to weak attraction between the layers, perfect basal cleavage planes parallel to (001) are created along which, upon mechanical stress, the mineral fractures preferentially. This rupture parallel to the ***a-b*** plane corresponds to delamination. This property also explains the lowest hardness in Mohs scale and the fact that the platelets slide apart at the slightest touch, giving talc its characteristic softness or slippery feel.

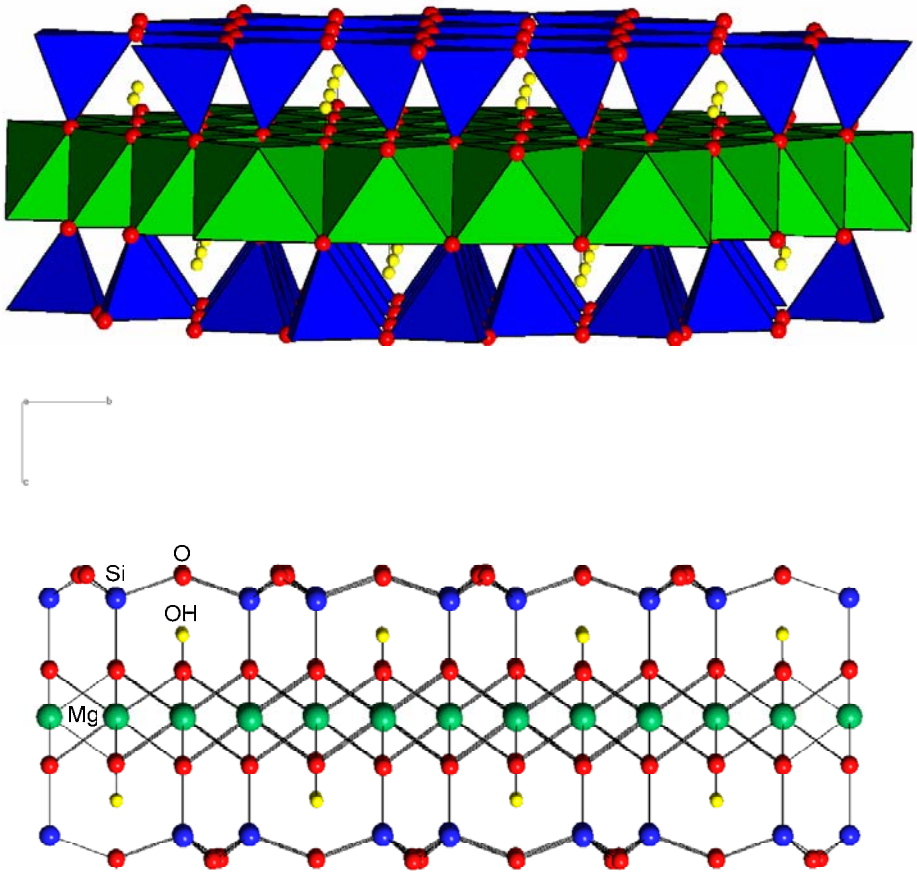


**Figure 1.9. The crystal structure of talc[3] in perspective view along 'a'[5] (1,0,0). The octahedral brucite ($Mg(OH)_2$) layer sandwiched between two tetrahedral sheets of silica can be observed. Upper picture: polyhedra representation; bottom picture: spheres representation.**

[5] The 'a' direction is perpendicular to the plane of the page.

Talc is also characterized by its crystallinity or relative platyness. The length of an individual talc platelet can vary from approximately 1 micron to over 100 microns depending on the conditions of formation of the deposit. It is this individual platelet size that determines talc's lamellarity. A highly lamellar or macrocrystalline talc will have large individual platelets, higher aspect ratio, lower surface area (usually lower than 10 $m^2/g$), and are much more difficult to micronize, whereas a microcrystalline talc will have small irregular platelets and are easily milled to very fine products of higher surface area (10–20 $m^2/g$) [58]. An electron micrograph illustrating the morphology of a macrocrystalline talc sample is shown in Figure 1.10.

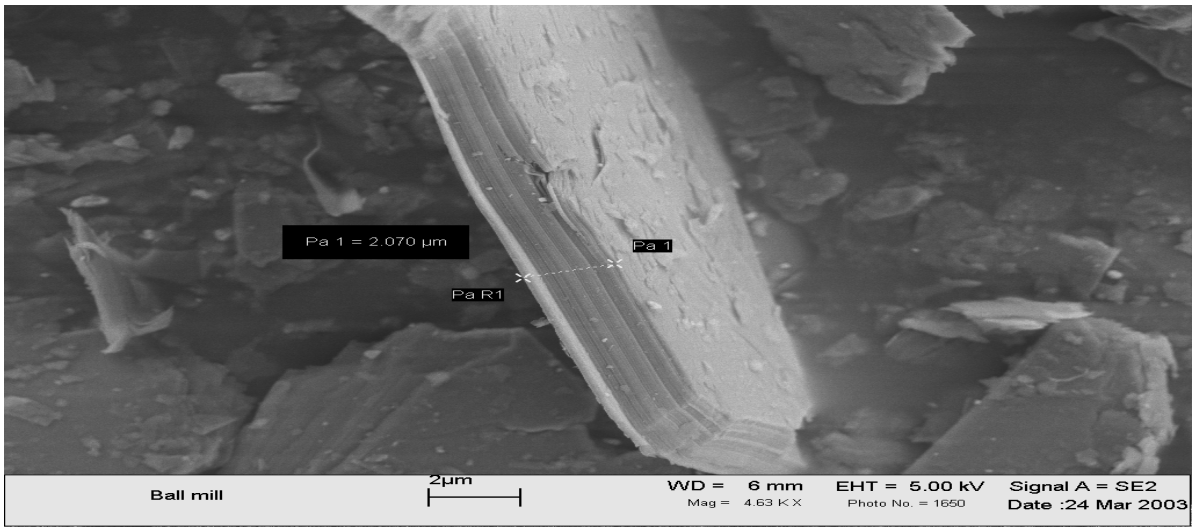


**Figure 1.10. Scanning electron micrograph (SEM) of talc powder showing the lamellar habit, consisting of stacks of individual sheet-like, or platy crystals held together by weak van der Waal's forces. The basal cleavage planes can also be observed (macrocrystalline talc product from Magnesita S.A., Brazil).**

A simple model was proposed by Likitalo [59] to quantitatively determine the difference in the morphology between distinct talc samples. The method is based on a comparison between the results obtained with two particles size distribution instruments, e.g. the Malvern (light scattering) and the Sedigraph (gravitational sedimentation). The equivalent spherical diameter derived from the analysis of anisometric particles is not the same when different physical phenomena are taken as the basis of measurement and agreement is only obtained when spherical particles are encountered. Thus, the relative form factor of particles having a similar shape can be

estimated by difference in particle size distribution using two different principles. The Lamellarity Index (L.I.) can then be defined as:

$$L.I. = \frac{D_{50}^{L} - D_{50}^{S}}{D_{50}^{S}} \tag{1.1}$$

where $D_{50}^{L}$ and $D_{50}^{S}$ are the average particle size measured by light scattering (L) and sedimentation (S), respectively. For spherical particles the L.I. approaches zero since $D_{50}^{L} \approx D_{50}^{S}$ and for anisodiametric particles the L.I. > 1. The greater the L.I., the greater the degree of lamellarity. Detailed information about the quantitative determination of shape factor of talc particles is given in Chapter 4.

Edge and basal surfaces of phyllosilicates vary greatly in reactivity due to the extreme anisotropy of phyllosilicate crystal structure [60]. In the case of talc, the external faces of the silica sheets, i.e. the basal planes, which account for almost the total surface area of the grinded mineral, do have neither hydroxyl groups nor active ions originated from broken bonds. Considering that usually talc has very little octahedral and tetrahedral isomorphic substitutions, the oxygen atoms from the (001) surfaces are bonded to two $Si^{4+}$ such that the sum of the bond valences from the cation to a basal oxygen is close to 2.0 [61]. As such, the basal oxygens are valence saturated and incapable of accepting hydrogen bonds [62]. These oxygens are, therefore, weak Lewis bases, the basicity coming from the lone pair of electrons which are directed away from the (001) surfaces. As a result the faces are apolar and oleophilic, hydrophobic and aerophilic, highly inert and non reactive [63]. The hydrophobicity of the basal plane also explains the natural floatability of talc [64] .

The hydrophilic sites are located on edges at talc lamellae and are characterized by broken covalent/ionic bonds, created due to the breakage of strong bonds perpendicular to the basal planes during comminution. For these cations (silicon and magnesium), the oxygens of adsorbed water molecules and hydroxyl groups fill out the coordination sphere. As mentioned before, the silanol groups have a weak acid

character whereas the magnesol are basic. It is believed that the edges of talc particles have a net acidic character judging from the fact that the isoelectric point (I.E.P.) of the mineral lies in the acidic region of pH (I.E.P. ≅ pH 3) [65].

As a mater of fact, surface anisotropy seems to be an inherent character of most hydrophobic solids [64]. This gives rise to particle-shape dependent properties of these materials, that is, particles of different shape might have different properties due to different ratios of hydrophobic-to-hydrophilic surface.

Lastly, talc can crystallize in two different crystal systems, monoclinic and triclinic [16]. For the monoclinic [66] and triclinic [67] unit cell the crystal structure parameters were determined as described in Table 1.4. However, to the best of our knowledge, the latter, represents the most recent review of talc's structure.

**Table 1.4. Structural parameters for talc**

| Unit cell parameters | Monoclinic From ref. [66] | Triclinic From ref. [67] |
|---|---|---|
| a (Å) | 5.28 | 5.2900 |
| b (Å) | 9.15 | 9.1730 |
| c (Å) | 18.92 | 9.4600 |
| $\alpha$ ($^o$) | 90.00 | 98.68 |
| $\beta$ ($^o$) | 100.15 | 119.90 |
| $\gamma$ ($^o$) | 90.00 | 85.27 |
| Z (nº of formula units per cell) | 4 | 2 |
| Space group | C2/c | P$\bar{1}$ |

### 1.7.2- Physical and optical properties

The color of natural talc varies. It can be white, gray, yellow, pale blue, or pale green [16]. It can also be pink and even black. It is colorless in thin section. Talc has a characteristic silvery or pearly luster. Upon grinding, however, all talcs yield a gray to white powder with varying degrees of dry brightness. The streak is white.

The crystal form of talc may be platelike (lamellar), foliated (leafy), fibrous (acicular), or massive. The particle shapes of commercial talcs are characteristic of their origin.

Talc exhibits perfect cleavage along (001) plane of symmetry, yielding flexible, slightly elastic, lamellae [16]. Pure talc is the softest known mineral. On the Mohs hardness scale of 1 to 10, talc is the standard for a hardness of 1 and has a “soapy or slippery” feel. Commercial talc products often tend to be harder than pure talc because of the presence of impurities such as calcite and tremolite. The measured density is in the range 2.58-2.83g/cm$^3$ and the calculated is 2.78 g/cm$^3$. It is infusible and inert to acids. The ambient pH of a 5% solids suspension of talc is 9.0 to 9.5.

Optically, talc is biaxial negative and exhibits three indices of refraction $\alpha$ = 1.54, $\beta$ = 1.58, $\gamma$ = 1.58 and $\delta$ = 0.05 [10]. The refractive indices increase with iron content. The $2V_\alpha$ angle experimentally ranges from 6$^o$ to 30$^o$. It appears smeared or poorly defined when viewed under crossed polars.

Talc is odorless. It is insoluble in water and in weak acids and alkalis. Although talc has a marked affinity for certain organic chemicals, it generally has very little chemical reactivity. It is neither explosive nor flammable.

Talc is a nonconductor of electricity. Therefore, it is used in the manufacture of high frequency electrical insulators.

Talc exhibits stability toward heat up to temperatures as high as 1650°F (≈900°C). It has low thermal conductivity and high resistance to thermal shock. Pure talc is thermally stable up to 930°C, and loses its crystalline bound water (4.8%) between 930 and 970°C [68], leaving an enstatite (anhydrous magnesium silicate) and cristobalite residue. Enstatite is significantly harder than talc with a Mohs hardness of 5-6 [69]. Most commercial talc products have thermal loss below 930°C on account of the presence of carbonates, which lose carbon dioxide at 600°C, and chlorite, which

loses water at 800°C. Talc's melting point is at 1500°C. Eq. (1.2) below describes the reaction that the mineral undergoes upon application of heat.

$$3\ MgO.4SiO_2.H_2O \xrightarrow{\Delta} 3\ MgSiO_3 + SiO_2 + H_2O \qquad (1.2)$$

(talc) (enstatite) (cristobalite)

Calculated Gibbs energy of formation of talc at 25°C and 1 atm pressure is -1319.4 ± 1.5 kcal/mol. Experimentally, the Gibbs energy of formation of talc at 25°C and 1 atm pressure is determined to be -1319 kcal/mol [70].

### 1.7.3- Chemistry

Talc is invariably a secondary mineral formed in preexisting rocks either directly from those rocks or through the introduction of new material. Due to the variety of ways in which the geological formation of talc is manifest, virtually every talc deposit is unique with regard to both chemistry and morphology [71]. Factors which characterize the commercial viability and final application of a talc deposit include:

- brightness and color
- platyness and crystallinity
- type and presence of nontalc minerals associated with genesis of the deposit

Nontalc minerals associated with commercial talc vary form deposit to deposit and commonly there does exist variation within the same deposit. The associated minerals may include calcite, quartz, magnesite, dolomite, chlorite and serpentine.

Most talc is very close to the ideal composition. In nature, however, it has at least traces of isomorphous substitution sites without exception. The only significant substitutions being $Fe^{2+}$ and $Fe^{3+}$ for $Mg^{2+}$, and concomitant $Al^{3+}$ for $Si^{4+}$ to maintain charge balance [9].

Micoud et al. thoroughly investigated a talc sample from the world famous Trimouns talc and chlorite deposit in the French Pyrénées using various spectroscopic methods [72]. They showed that minor substitutions causing a deficiency of charge in the tetrahedral sheet were compensated by an excess of charge in the octahedral sheet, ensuring electro-neutrality of the structure. On the other hand, Brady and co-workers described that minor substitutions of $Al^{3+}$ or $Fe^{3+}$ for $Si^{4+}$ in the tetrahedral sheet would give rise to a small permanent (non-pH dependent) negative charge on the Si basal plane. More recently, Petit *et al.* investigate the crystal chemistry of various talc samples from different origins [73]. The complexity and variety of possibilities of substations make it impossible to draw broad conclusions about talc's chemistry. A detailed discussion on the chemistry of crystalline clay minerals can be found in the work of Newman [74].

## 1.8- Talc samples characterization - experimental details

**Magnesita S.A.**, a Brazilian company dedicated to the manufacture of an extensive line of refractories and processing of industrial minerals, provided the talc used in this investigation. Eight samples were chosen targeting primarily to cover a broad range of particle sizes, going from coarse to nano-sized particles, using different grinding technologies. They all originated form the Cabeceiras Mine located in city of Brumado, State of Bahia, Brazil. The chemical, mineralogical and physical characterization of the samples are described in Table 1.5 a/b. All the analyses, except the SEM morphological characterization, were done cooperatively in the Research and Development Center of Magnesita S.A. at Contagem and in the Laboratory for Quality Control at Brumado. Some analyses were done in triplicates and in this case the average values are presented and the standard deviations are shown in parentheses.

In order to protect the proprietary information of Magnesita, the samples are hereafter identified from A to H. For the same reason, the grinding technology used to produce each sample could not be disclosed.

**Qualitative mineralogical characterization:** Diffraction patterns were obtained using a Philips X-ray diffractometer (Model PW 1730/10) with a graphite monochromator and Cu K$\alpha$ radiation ($\lambda$ = 1.5418 Å) at 40 kV, 40 mA and at a scanning rate of $2^{o}$ at $2\theta$ $min^{-1}$ at 295 K.

**Morphological characterization:** The LEO 1550 Field Emission Scanning Electron Microscope (FESEM) was used for this purpose. Prior to the analysis, the samples were coated with 8 nm thick Au-Pd film. The accelerating voltage used which was 5kV. This characterization was done at Virginia Tech.

**Chemical analysis:** Chemical analysis was carried out using a sequential X-ray fluorescence spectrometer MagiX PRO (Philips). X-ray tube: Rh - 4 kW.

**Density:** A helium pycnometer Stereopycnometer SPY-3 (Quantachrome Instruments) was used to determine the true density.

**Specific surface area (SSA):** The BET specific surface area was determined by means of a low-temperature adsorption of nitrogen. Nitrogen adsorption isotherms at 77 K were determined volumetrically using a Quantasorb 8-17 analyzer (Quantachrome Instruments).

**Particle size distribution (PSD):** The PSD for the different samples was determined by means of two different equipments:

- for the gravitational sedimentation method the Sedigraph 5100 (Micromeritics, GA, USA) was used to cover the particle size range from about 0.5 µm to 100 µm;
- for the laser diffraction method the Malvern Mastersizer S (Malvern, UK) was used to cover the particle size range from about 0.05 µm to 900 µm.

Prior to the particle size analysis, the particles were thoroughly dispersed in water by the aid of dispersing agent (sodium hexametaphosphate) and ultrasonic disruptor (200 W, 2 minutes). All the analytical results and additional information about particle size characterization are given in Chapter 4.

**Whiteness and yellowness index:** The spectrophotometer (Datacolor, Elrepho 2000) was used for these determinations. MgO p.a. was chosen as a 100% whiteness reference material. The whiteness (FMY-green filter) was determined at 457 nm.

## 1.9- Scope of work

The first part of this project is to investigate the surface free energies of talc using the modern acid-base theory. This is divided into two chapters. A theoretical review of the thermodynamic aspects of solid's surface is covered in Chapter 2 that follows. The experimental results of contact angle and the surface free energy parameters and components, using mainly thin layer wicking technique, are given in Chapter 3. Also in this chapter, other techniques for contact angle determination on powdered and flat surfaces are also presented and discussed. In Chapter 4 two particle size distribution techniques, namely gravitational sedimentation and laser diffraction, are used to quantitatively determine the aspect ratio of anisometric talc particles. In Chapter 5, flow microcalorimetry (FMC) is used to assess the percentage of hydrophilic and hydrophobic sites on talc surface and, by combining FMC with thin layer wicking, the individual surface components at basal planes and edge surfaces are independently determined. Finally, suggestions for future work are presented.

**Table 1.5a. Chemical and mineralogical characterization of the talc samples tested**

| samples → | A | B | C | D | E | F | G | H |
|---|---|---|---|---|---|---|---|---|
| **CHEMICAL AND MINERALOGICAL ANALYSIS** | | | | | | | | |
| **Chemical Analysis (% w/w)** | | | | | | | | |
| **( L.O.I. )** | 4.83 | 4.83 | 7.34 | 4.88 | 5.75 | 6.09 | 6.67 | 6.96 |
| **$SiO_2$** | 63.50 | 63.07 | 59.39 | 62.91 | 61.73 | 61.24 | 60.43 | 59.88 |
| **$TiO_2$** | 0.00 | 0.01 | 0.03 | 0.02 | 0.02 | 0.13 | 0.30 | 0.47 |
| **$Al_2O_3$** | 0.17 | 0.36 | 0.57 | 0.49 | 0.53 | 0.73 | 0.73 | 0.71 |
| **$Cr_2O_3$** | 0.00 | 0.00 | 0.01 | 0.00 | 0.00 | 0.01 | 0.00 | 0.00 |
| **$Fe_2O_3$** | 0.22 | 0.24 | 0.29 | 0.28 | 0.23 | 0.22 | 0.23 | 0.22 |
| **MnO** | 0.00 | 0.00 | 0.00 | 0.00 | 0.00 | 0.00 | 0.00 | 0.00 |
| **CaO** | 0.00 | 0.00 | 0.46 | 0.04 | 0.08 | 0.10 | 0.17 | 0.21 |
| **MgO** | 31.32 | 31.49 | 31.91 | 31.38 | 31.67 | 31.48 | 31.47 | 31.55 |
| **Moisture (%)** | n.d. | n.d. | 0.29 | 0.19 | 0.75 | 0.32 | 0.69 | 0.89 |
| **D.R.X Mineralogical phases (qualitative)** | n.d. | n.d. | Talc Magnesite Quartz Chlorite | Talc | Talc Magnesite Quartz | Talc Magnesite Quartz | Talc Magnesite Quartz | Talc Magnesite Quartz Rutile |
| **Free silica (%)** | n.d. | 0.07 | 0.53 | None | 0.33 | 1.64 (0.06) | 1.28 (0.05) | 0.76 (0.02) |

**Table 1.5b. Physical characterization of the talc samples tested**

| samples → | A | B | C | D | E | F | G | H |
|---|---|---|---|---|---|---|---|---|
| **PHYSICAL ANALYSIS** | | | | | | | | |
| **Specific gravity (g/cm³)** | 2.84 | 2.88 | 2.96 (0.03) | 2.99 (0.02) | 3.02 (0.05) | 2.96 | 2.98 | 3.18 |
| **Specific surface area (BET) (m²/g)** | 1.14 | 9.28 | 10.88 (0.35) | 9.29 (0.53) | 26.32 (1.08) | 13.31 (0.37) | 24.64 (0.61) | 29.35 (0.51) |
| **Specific surface area (Blaine) (cm²/g)** | n.d. | n.d. | 20,721 | 38,279 | 43,046 | 41,421 | 61,313 | 61,987 |
| **Solubles in HCl** | n.d. | 0.98 | 3.64 | 0.52 | 2.22 | 2.32 | 4.06 | 5.00 |
| **Witheness FMY (%)** | 98.05 | 97.54 | 94.51 | 94.69 | 96.42 | 96.36 | 96.75 | 96.88 |
| **Yellowness index (%)** | 0.30 | 0.29 | 2.38 | 5.54 | 1.93 | 1.97 | 1.53 | 1.39 |
| **Loose density (g/cm²)** | n.d. | n.d. | 0.24 | 0.12 | 0.12 | 0.10 | 0.09 | 0.08 |
| **Tapped density (g/cm²)** | n.d. | n.d. | 0.83 | 0.50 | 0.50 | 0.51 | 0.40 | 0.38 |

**Note: n.d. – not determined.**

## 1.10- References


1. Adamson, A.W., *Physical Chemistry of Surfaces*. 1990, New York: Wiley-Interscience.

2. Good, R.J. and C.J. van Oss, *The modern theory of contact angles and the hydrogen bond components of surface energies*, in *Modern Approaches to Wettability*, M.E. Schrader and G.I. Loeb, Editors. 1992, Plenum Press: New York.

3. van Oss, C.J. and R.F. Giese, *Colloid and surface properties of clay and related minerals*. 2002, New York: Marcel Dekker.

4. Wills, B.A., *Mineral Processing Technology*. 6th ed. 1997, Cornwall: Butterworth Heinemann.

5. Kauffman, S.H.*, et al.*, *The preparation and classification of high aspect ratio mica flakes for use in polymer reinforcement.* Powder Technology, 1974. **9**: p. 125-133.

6. Lohmander, S., *Influence of shape and shape factor of pigment particles on the packing ability in coating layers.* Nordic Pulp and Paper Research Journal, 2000. **15**(4): p. 300-305.

7. Lohmander, S., *Influence of a shape factor of pigment particles on the rheological properties of coating.* Nordic Pulp and Paper Research Journal, 2000. **15**(3): p. 231-236.

8. Bharadwaj, R.K., *Modeling the barrier properties of polymer-layered silicate nanocomposites.* Macromolecules, 2001. **34**: p. 9189-9192.

9. Gaines, R.V.*, et al.*, *Dana's New Mineralogy*. 8th ed. The System of Mineralogy of James Dwight Dana and Edward Salisbury Dana. 1997, New York: John Wiley&Sons. 1437 - 1442.

10. Perkins, D., *Mineralogy*. 2nd ed. 2002, New Jersey: Prentice Hall. 315.

11. Katz, H. and J.V. Milewski, *Handbook of Fillers for Plastics*. 1987, New York: Van Nostrand Reinhold. 216-231.

12. Virta, R.L., *Talc and Pyrophyllite*. 2002, U.S. Geological Survey.

13. Guggenheim, S. and R.R. Marin, *Definition of Clay and Clay Mineral: Joint Report of The AIPEA Nomenclature and CMS Nomenclature Committees.* Clays and Clay Minerals, 1995. **43**(2): p. 255-256.

14. Yariv, S., *Wettability of Clay Minerals*, in *Modern Approaches to Wettability*, M.E. Schrader and I.L. George, Editors. 1992, Plenum Press: New York. p. 279-326.

15. Bailey, S.W., *Introduction*, in *Hydrous Phyllosilicates*. 1991, Mineralogical Society of America: Chelsea. p. 1-8.

16. Deer, W.A.*, et al.*, *Rock-Forming Minerals - Sheet Silicates*. 1st ed. Vol. 3. 1962, New York: Longmans.

17. Pauling, L., *The principles determining the structure of complex ionic crystals.* Journal of the American Chemical Society, 1929. **51**(4): p. 1010-1026.

18. Pauling, L., *The structure of the micas and related minerals.* Proceedings of the National Academy of Sciences, USA, 1930. **16**(2): p. 123-129.

19. Pauling, L., *The structure of the chlorites.* Proceedings of the National Academy of Sciences, USA, 1930. **16**(9): p. 578-582.

20. Sposito, G., *The surface chemisty of soils*. 1984, Oxford University Press.

21. Sparks, D.L., *Environmental Soil Chemistry*. 1995, San Diego: Academic Press. 23-51.

22. Sposito, G.*, et al.*, *Surface geochemistry of the clay minerals.* Proceedings of the National Academy of Sciences, USA, 1999. **96**(7): p. 3358-3364.

23. *Internet Glossary of Soil Science Terms*. 2001, Soil Science Society of America.

24. Velde, B., *Origin and Mineralogy of Clays*. 1995, Berlin: Springer-Verlang. 8-42.

25. Shannon, R.D., *Revised Effective Ionic Radii and Systematic Studies of Interatomic Distances in Halides and Chalcogenides.* Acta Crystallographica, 1976. **A32**: p. 751-767.

26. Brown, G., *Crystal structures of clay minerals and related phyllosilicates.* Philosophical Transactions of the Royal Society of London. Series A, Mathematical and Physical Sciences, 1984. **311**(1517): p. 221-240.

27. Guven, N., *Smectites*, in *Hydrous Phyllosilicates*, S.W. Bailey, Editor. 1991, Mineralogical Society of America: Chelsea.

28. Schoonheydt, R.A., *Clay mineral surfaces*. Mineral Surfaces, ed. D.J. Vaughan and R.A.D. Pattrick. Vol. 5. 1995, London: Chapman & Hall. 303-327.

29. Mermut, A.R., *Layer charge characteristics of 2:1 silicate clay minerals*. CMS workshop lectures, ed. A.R. Mermut. Vol. 6. 1994, Aurora: The Clay Minerals Society. 106-122.

30. McBride, M.B., *Environmental Chemistry of Soils*. 1994, New York: Oxford University Press.

31. Jensen, W.B., *The Lewis Acid-Base Concepts*. 1980, New York: John Wiley and Sons.

32. Lindgreen, H., *et al.*, *Ultrafine particles of North Sea illite/smectite clay minerals investigated by STM and AFM.* American Mineralogist, 1991. **76**: p. 1218-1222.

33. Henderson, G.S., *et al.*, *Atomic force microscopy studies of layer silicate minerals.* Colloids and Surfaces A: Physicochemical and Engineering Aspects, 1994. **87**(3): p. 197-212.

34. Gunter, W.D. and Z. Zhou, *The nature of the surface charge of kaolinite.* Clays and Clay Minerals, 1992. **40**(3): p. 365-368.

35. Schrader, M.E. and S. Yariv, *Wettability of clay minerals.* Journal of Colloid and Interface Science, 1990. **136**(1): p. 85-94.

36. Guggenheim, S. and J.H. Lee, *Single crystal X-ray refinement of pyrophillite-1 Tc.* American Mineralogist, 1981. **66**: p. 350-357.

37. Guggenheim, S. and J.C. Lin, *The crystal structure of a Li, Be-rich brittle mica: a dioctahedral-trioctahedral intermediate.* American Mineralogist, 1983. **68**: p. 130-142.

38. Persello, J., *Surface and Interface Structure of Silicas*, in *Adsorption on Silica Surfaces*, E. Papirer, Editor. 2000, Marcel Dekker: New York. p. 311.

39. Yariv, S., *The effect of tetrahedral substitution of Si by Al on the surface acidity of the oxygen plane of clay minerals.* International Reviews in Physical Chemistry, 1992. **11**(2): p. 345-375.

40. Garfinkel-Shweky, D. and S. Yariv, *The Determination of Surface Basicity of the Oxygen Planes of Expanding Clay Minerals by Acridine Orange.* Journal of Colloid and Interface Science, 1997. **188**(1): p. 168-175.

41. Liebau, F., *Structural chemistry of silicates - structure, bonding and classification*. 1985, Berlin: Springer-Verlag.

42. Noguera, C., *Physics and chemistry at oxide surfaces*. 1st ed. 1996, New York: Cambridge University Press.

43. Stumm, W., *Chemistry of the solid-water interface: processes at the Mineral-Water and Particle-Water Interface in Natural Systems*. 1991: Wiley.

44. Dugger, D.L.*, et al.*, *The Exchange of Twenty Metal Ions with the Weakly Acidic Silanol Group of Silica Gel.* Journal of Physical Chemistry, 1964. **68**(4): p. 757 - 760.

45. Hair, M.L. and W. Hertl, *Acidity of surface hydroxyl groups.* Journal of Physical Chemistry, 1970. **74**(1): p. 91-94.

46. Hiemstra, T.*, et al.*, *Intrinsic Proton Affinity of Reactive Surface Groups of Metal (Hydr)oxides: The Bond Valence Principle.* Journal of Colloid and Interface Science, 1996. **184**(2): p. 680-692.

47. Hiemstra, T. and W.H.V. Riemsdijk, *On the relationship between surface structure and ion complexation of oxide-solution interfaces*, in *Encyclopedia of Surface and Colloid Science*, P. Somasundaran, Editor. 2002, Marcel Dekker: New York. p. 3773-3799.

48. Hiemstra, T.*, et al.*, *Multisite proton adsorption modeling at the solid/solution interface of (hydr)oxides: a new approach.* Journal of Colloid and Interface Science, 1989. **133**(1): p. 91-104.

49. Tanabe, K.*, et al.*, *New Solids Acids and Bases*. Studies in Surface Science and Catalysis, ed. B. Delmon and J.T. Yates. Vol. 51. 1989, Tokyo: Elsevier. 21.

50. Schwarz, J.A., *Acid-base behavior of oxide and related surfaces*, in *Encyclopedia of Surface and Colloid Science*, P. Somasundaran, Editor. 2002, Marcel Dekker: New York. p. 64-73.

51. Gehring, A.U.*, et al.*, *Octahedral sites in talc revisited: and EPR study.* Clay Minerals, 1988. **33**: p. 661-664.

52. Rayner, J.H. and G. Brown, *The Crystal Structure of Talc.* Clays and Clay Minerals, 1973. **21**: p. 103-114.

53. Bleam, W.F., *Electrostatic potential at the basal (001) surface of talc and pyrophyllite as related to tetrahedral sheet distortions.* Clays and Clay Minerals, 1990. **38**(5): p. 522-526.

54. Ward, W. and J.M. Phillips, *Calculated lamellar binding I. van Der Waals bonding in talc and pyrophyllite.* Surface Science, 1971. **25**: p. 379-384.

55. Giese, J., R. F., *The electrostatic interlayer forces of layer structure minerals.* Clays and Clay Minerals, 1978. **26**(1): p. 51-57.

56. Okuda, S., *et al. Negative surface charges of pyrophyllite and talc*. in *International Clay Conference*. 1969.

57. Giese, J., R. F., *Interlayer bonding in talc and pyrophyllite.* Clays and Clay Minerals, 1974. **23**: p. 165-166.

58. Zazenski, R., *et al.*, *Talc: Occurrence, Characterization, and Consumer Applications.* Regulatory Toxicology and Pharmacology, 1995. **21**: p. 218-229.

59. Likitalo, M., *Talc*, in *Pigment Coating and Surface Sizing of Paper*, E. Lehtinen, Editor. 2000, Finnish Paper Engineers' Association and TAPPI. p. 106-119.

60. Giese, J., R. F., *et al.*, *The surface free energies of talc and pyrophillite.* Physics and Chemistry of Minerals, 1991. **17**: p. 611-616.

61. Bleam, W.F., *The nature of cation-substitution sites in phyllosilicates.* Clays and Clay Minerals, 1990. **38**(5): p. 527-536.

62. Bickmore, B.R., *et al.*, *AB initio determination of edge surface structures for dioctahedral 2:1 phyllosilicates: implications for acid-base reactivity.* Clays and Clay Minerals, 2003. **51**(4): p. 359-371.

63. Skipper, N.T., *et al.*, *Computer calculation of water-clay interactions using atomic pair potentials.* Clay Minerals, 1989. **24**: p. 411-425.

64. Fuerstenau, D.W., *et al.*, *On the native floatability and surface properties of naturally hydrophobic solids.* AIChe Symposium Series, 1975. **71**(150): p. 183-188.

65. Fuerstenau, M.C., *et al.*, *Role of hydrolyzed cations in the natural hydrophobicity of talc.* International Journal of Mineral Processing, 1988. **23**(3-4): p. 161-170.

66. Lima-de-Faria, J., *Talc*, in *Structural Mineralogy - an introduction*. 1994, Kluwer: The Netherlands. p. 227-228.

67. Perdikatsis, B. and H. Burzlaff, *Strukturverfeinerung am Talk.* Zeitschrift fur Kristallographie, 1981. **156**: p. 177-186.

68. Wesolowski, M., *Thermal decomposition of talc: a review.* Thermochimica Acta, 1984. **78**: p. 395-421.

69. Clark, R.J. and W.P. Steen, *Talc in polypropylene*, in *Handbook of polypropylene and polypropylene composites*, H.G. Karian, Editor. 2003, Marcel Dekker: New York. p. 281-309.

70. Bricker, O.P., *et al.*, *The Stability of Talc.* American Mineralogist, 1973. **58**(64-72).

71. Piniazkiewicz, R.J., *et al.*, *Talc*, in *Industrial Minerals and Rocks*, D.D. Carr, Editor. 1994, Society for Mining, Metallurgy and Exploration: Colorado. p. 1049-1069.

72. Martin, F., *et al.*, *The structural formula of talc from the Trimouns deposit, Pyrénées, France.* The Canadian Mineralogist, 1999. **37**(4): p. 997-1006.

73. Petit, S., *et al.*, *Crystal-chemistry of talc: A near infrared (NIR) spectroscopy study.* American Mineralogist, 2004. **89**: p. 319-326.

74. Newman, A.C.D. and G. Brown, *The chemical constitution of clays*, in *Chemistry of Clays and Clay Minerals*, A.C.D. Newman, Editor. 1987, Longman Scientific&Technical: London. p. 1-128.